DESIGN OF A PROTOTYPE UNMANNED LIGHTER-THAN-AIR PLATFORM FOR REMOTE SENSING:

(Article begins on next page)

17 August 2022

DESIGN OF A PROTOTYPE UNMANNED LIGHTER-THAN-AIR PLATFORM FOR REMOTE SENSING:
STRUCTURAL DESIGN AND OPTIMIZATION

C. Surace[1,3], R. Roy[2], M. Civera[2,3], D. Allaio[2], R. Barbieri[2], A. Grava[2], R. Tufilli[2], & P. Gili[2,3]

[1] Department of Structural, Geotechnical and Building Engineering, Politecnico di Torino, Turin, Italy
[2] Department of Mechanical and Aerospace Engineering, Politecnico di Torino, Turin, Italy
[3] Interdipartimental Responsible Risk Resilience Centre (R3C), Politecnico di Torino, Turin, Italy

Abstract

This work presents the structural design of a new Remotely Piloted Aircraft System (RPAS) concept for land survey applications. The RPAS Lighter-Than-Air (LTA) platform is equipped with a thrust vectoring control system made of six propellers attached to a single-rib exoskeletal load-bearing structure. The load-bearing structure is optimized to minimize structural mass, maximize payload capability, and meet the airship's operational requirements. A finite element model of the load-bearing structure was developed and analyzed under normal operating conditions of the airship, such as mid-air hovering and parking. Additionally, various failure cases, such as crash landing and control system failure, leading to haphazard operation of the propellers, were considered to simulate extreme load conditions on the airship exoskeletal structure. Airship slenderness was also considered an important design parameter and was optimized to maximize aerodynamic performance. A twin paper describes the other non-structural aspects of the airship design.

Keywords: Airship Design; Finite Element modelling; Structural Analysis; Remotely Piloted Aircraft System; Lighter-Than-Air Platform.

1. Introduction

Airships are a particular class of aircraft that uses lighter-than-air (LTA) gases to generate vertical lift rather than relative motion with respect to external air. They can be classified into:

- Rigid airships, which are characterized by an internal frame made of suitable material, typically Aluminium, which determines their shape, and numerous cells filled with LTA gases. The rigid structure they are equipped with is ideal for attaching sub-units, such as the gondola or the propellers.
- Floppy airships (or Blimps) have the characteristic of maintaining their spindle shape not owing to a rigid structure, but by employing the overpressure of gas contained in the casing in comparison to the external gas. The absence of a frame facilitates an increase in the payload, but also less stability. This category also includes hot air airships that can presently achieve excellent internal pressurization due to the advent of more resistant fabrics and new technology.
- Semi-rigid airships, which are instead characterized by a single keel reticular truss, to which the actual balloon is longitudinally fixed. The envelope maintains its shape partly by overpressure, partly thanks to the truss that runs from bow to stern, and which acts as a support for the nacelle, the load, the engines and the equipment. They present an intermediate between rigid and limp airships.

The most used LTA gases are hydrogen and helium, due to their low molecular weight. Hydrogen guarantees greater thrust at the same volume (due to its lower density) and has a lower cost than helium but requires extreme care in handling to avoid explosions or fires. In recent years, studies have been carried out on the use of other gases, such as hot air, methane, and ammonia, although they produce a lower thrust than the previous choices. A comparison of properties between these gases is

reported in Table 1.

Table 1 – Properties of gases commonly used for airship design.

	Specific weight * [kg/m^3]	Thrust **[N]
Hydrogen	0.0899	11.79
Helium	0.1786	10.92
Ammonia	0.7598	5.23
Methane	0.7157	5.654

* at 273.15 K and 1 atm
** referred to the volume of the envelope; calculated in dry air at 273.15 K and 1 atm

Despite the primary requirement that the envelope is of a tapered shape to reduce air resistance and increase controllability, in recent years, research has been carried out to study the use of unconventional airship shapes, like spherical. Although such a shape leads to much greater friction than the standard shape, it has numerous advantages: it has the lowest possible surface to volume ratio, and therefore the maximum buoyancy. Also, it does not require forward movement to land or lift. Other shapes developed incorporated aerodynamic surfaces to generate aerodynamic thrust and improve handling. Lenticular shapes have been developed along this line, with multiple hulls or 'winged envelopes'. A category worthy of mention is the so-called hybrid airships: aircraft that partly exploit the thrust generated by light gases and partly the aerodynamic thrust generated by their shape. They can be considered as a hybrid between a traditional aircraft (such as a helicopter or a plane) and an airship. Such aircraft can carry significantly greater loads than traditional airships and are much less sensitive to atmospheric conditions.

The envelope of the airship must meet numerous requirements:

- Resistance to chemical-physical degradation
- Shielding from solar radiation
- Low weight
- Resistance to temperature changes
- High flexibility
- Low permeability to minimize gas losses.

An optimal solution meeting these requirements is a multilayer laminated fabric in which the individual functions are performed by different layers. Four main layers can be identified:

- A load-resistant layer, characterized by high specific resistance, high tear resistance and high flexibility,
- A gas-impermeable layer, with low gas permeability,
- A protective layer against atmospheric agents, including high resistance to UV rays, humidity, and environmental degradation,
- An insulating layer characterized by low conductivity and used primarily with solar cells on the envelope surface.

The details of the proposed concept and design will be outlined in the next sections. For the sizing of the overall structure, a multidisciplinary design approach was followed. This is described in detail in a twin paper [1].

2. Proposed Concept for a Non-Conventional LTA Platform

Survey and monitoring applications have some specific requirements that are easily satisfied by an unmanned airship over all other types of aircraft. Low operational noise, low environmental impact, and hovering capability make airships perfect candidates for long time survey missions even above urban centres [2].

In the present work, the shape of the LTA platform has been selected as symmetric and ellipsoidal, in lieu of the classical raindrop shape (see Figure 1). A primary reason behind this choice is the serpentine path followed by the airship during monitoring operations so that it can easily proceed in both directions without requiring a U-turn. The main structure is represented by an elliptic rib, where propellers and the gondola are mounted [3].

The payload on-board can be divided into two main categories:

- Detection payload: LiDAR system and digital, infrared, and hyperspectral cameras,
- Control and manoeuvre systems: including systems for remote flight and communication with a ground station.

Rather than aerodynamic surfaces, thrust vectoring of the propellers is chosen as the manoeuvring and translation system of the airship due to its high efficiency at low velocities [4]. Four orientable propellers are symmetrically placed above and below the main rib for executing nose-dive or pitch-up manoeuvres. Two fixed vertical axis propellers are placed at the extreme ends of the ellipsoid major axis and these assist the lifting gas (usually helium) in executing vertical descent or ascent manoeuvres.

Electric power for payload and propulsion systems is provided by an energy system consisting of Fuel cells and batteries; these, along with the propulsion system, are discussed in detail in the companion paper [1].

Figure 1 - 3D rendering of the proposed airship concept.

3. Structural Design

The present section discusses the various aspects of the structural design of the semi-rigid airship proposed in Section 2. As the main structural frame of the airship is constituted by an elliptical rib, the structural design of the airship focuses on designing and sizing the rib to withstand the various loads and guarantee acceptable structural resistance during airship manoeuvres or more critical flight conditions. In the present design, a bi-cell cross-section is chosen for the main rib and is presented in Figure 2.
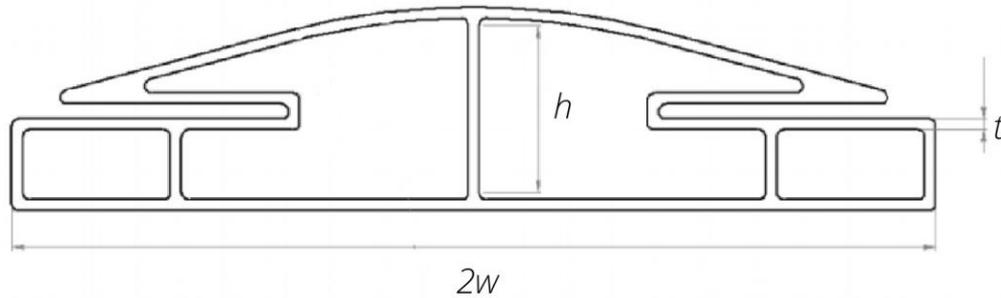
Figure 2 - Illustration of the main geometrical parameters of the section.

The chosen cross-section, derived from earlier works [5], is symmetric with two recesses, to facilitate the attachment with the airship's external envelope, and with two small internal cells for routing electrical wiring all along the rib. The key geometrical parameters used for designing the rib cross-section are:

- half-width w
- height h
- thickness t

In the present analysis, it is assumed that h and t are functions of the half-width w, i.e., $t=w/40$ and $h=w/2$. Hence, the half-width becomes the only independent parameter.

The structural design of the airship is carried out by considering some sample lengths for the major axis of the ellipsoid, $2a$. For each airship length, the design procedure attempts to find a value of w such that the airship maintains structural integrity and the strains and stresses developed on the structure are within certain limit values. However, an indiscriminate increase in the value of w consequently increases the total weight of the airship and impedes airship performance. The iterative procedure used for structural design is discussed in detail in the next sections. The final aim is to identify the airship dimensions that simultaneously satisfy structural requirements and facilitate hovering capability.

3.1 Airship Slenderness

An important factor to consider in airship design is its slenderness, which is defined as the ratio between airship length (L) and maximum diameter (d). Two aspects were considered when defining the geometric slenderness of the airship:

- The ratio between the airship weight and the aerostatic thrust,
- The aerodynamic resistance.

Concerning the first aspect, it was found that for constant airship length, as the slenderness increases, the ratio between weight and thrust increases monotonously. For estimating the aerodynamic resistance of the airship, Hoerner's formula was used to calculate the drag coefficient as a function of airship slenderness (see Figure 3). This formula provides a reasonable approximation for the drag coefficient for an ellipsoidal airship in an incompressible fluid. This relationship shows that the drag coefficient has a minimum for a slenderness value of 4.65.
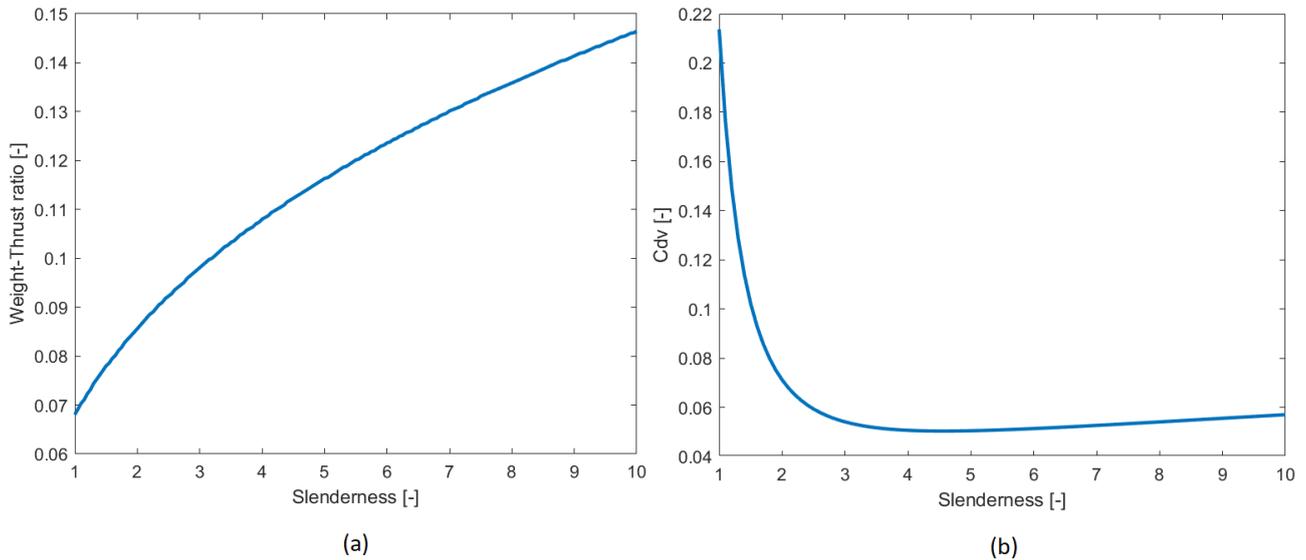
4

Figure 3 – Variation of (a) weight to thrust ratio, and (b) drag coefficient, as a function of slenderness.

To determine the optimal slenderness, the missions carried out by the airship were taken into account. The relationship between the weight of the airship and the aerostatic thrust influences the hovering phase, while the aerodynamic drag affects the cruise flight. Considering missions of different nature in terms of distribution between the hovering phase and the cruising phase, and considering different speeds for both phases, it was found, through the use of a genetic optimization algorithm implemented in MATLAB, how slenderness is more influenced by the cruise flight and therefore its optimal value is within the range of 3 to 4.6.

3.2 Airship weights

To perform a structural analysis of the proposed airship, the loads on the structure have to be addressed. The following list (summed up in Table 2) contains the most relevant loads for the analysis:

- The rib: given that the rib is the main structural member, the weight can be determined once the airship length, rib cross-section and building material are specified,
- The onboard systems: it is difficult to estimate, as the onboard systems are not directly addressed in this study. The weight is expected to be a function of mission requirements and mission operations and is also expected to increase with the airship dimensions. Therefore, a precise value cannot be calculated, but a sensible estimate is assumed in accordance with the mean dimensions of a conventional LTA platform,
- The propulsive system [4]: constitutes the weight of electric motors and propellers. Electric motor dimensioning is related to the needed cruise power and is extremely sensitive to the cruise speed V. While aerodynamic drag is proportional to V^2, the power to sustain such speed is proportional to V^3,
- The landing gear: it is difficult to estimate during initial airship sizing and is neglected in the present study,
- The payload: it is not part of the main airship operational system, but rather facilitates the execution of mission requirements. Payload weight depends strictly on the mission typology. As the study was focused on an LTA platform for environmental monitoring, an accurate estimate of 100 kg for the payload weight is used.

5

Table 2 – Weights of various airship subsystems relevant for the structural analysis.

Component	Location	Weight [kg]
Propellers (x 6)	Concentrated on rib	25 (each)
On-board systems	Concentrated on belly	300
Payload	Concentrated on belly	100

3.3 Structural Material

Structural mass depends on the material used for manufacturing the rib. To comply with the aerospace industry trends, the material of choice must be performant and lightweight at the same time. Materials with high specific properties best fit the following requirements:

- Strength: structure should resist external loads without incurring structural failures,
- Stiffness: structure should not deform excessively when contingency loads are applied,
- Weight reduction: the materials of choice should have high mechanical resistance but still have relatively low density,
- Moreover, the cost sustainability of the project must also be met. However, this issue does not fall within the scope of this paper.

Amongst the metal alloys, the most natural choice is Aluminium; it is commonly used in the aerospace industry and is appreciated for its relatively high stiffness to density ratio. An Aluminium-Copper (Al-Cu) alloy of the 2024T3 series is chosen for the present study and its material properties have been detailed in Table 3 [6].

As an alternative to metal alloys, a carbon/epoxy composite material (made of a polymeric matrix and high strength carbon fibre reinforcements) is also considered. In particular, the High Modulus (HM) series was adopted [7]. It has a very high mechanical performance with a lower density (and thus, weight) compared to metal alloys and has excellent stiffness properties. Stiffness is an essential quality for an LTA vehicle design to prevent excessive deformations once the rib is loaded. Structural deformations should be minimized since they degrade the LTA body slenderness leading to increased aerodynamic drag. Hence, the HM series was chosen instead of the HT (High tenacity) series, which generally would require the rib to be slightly oversized to ensure good stiffness levels.

These two options represent the best candidates as selected from a range of potential alternatives, including classic or more advanced structural materials such as e.g. Fiber Reinforced Polymeric composites, which are however subject to manufacturing defects [8, 9].

Table 3 – Mechanical properties of the Al-Cu alloy and carbon/epoxy composite.

Series 2024T3 Al-Cu alloy		HM Carbon/epoxy composite			
Density [kg/m³]	2780	Density [kg/m³]	1500	G_{12} [GPa]	3
Elastic modulus (E) [GPa]	73	E_1 [GPa]	157	Ultimate Tensile Stress [MPa]	900
Poisson's ratio [-]	0.3	E_2 [GPa]	8	Ultimate Compressive Stress [MPa]	675
Yield stress [MPa]	345	Poisson's ratio [-]	0.3		

3.4 Airship Operations

Among all the configurations and manoeuvres that an airship can perform, it is useful to analyze the most significant flight conditions for a primary structural evaluation. In this paper, three principal groups of flight conditions are discussed:

- Hovering and cruise flight,
- Parking and crashing,
- Manoeuvres with thrusters and failure of the thrust control system.

As the initial step, it is important to study the structural response in normal flight conditions, like hovering and cruise flight. Although these are not the most structurally demanding cases, they must be taken into account for a long period of permanence during flight. Short period manoeuvres like parking, nosedive, and thrust control system failure are considered as the next step.

3.5 Design Failure Conditions

The limiting values of stress and strain, depending on the material used, serves as the primary design failure condition for the envisioned airship structure. For a specific rib design, the stresses and strains developed on the structure should not exceed these material limits to maintain structural integrity. The maximum allowable stress for the two materials is described below (see Table 4),

- Al-Cu 2024T3 alloy: the limiting stress is governed by the yield point of the material. A suitable Safety Factor (SF) is also introduced with a value of 1.5 (typical for aeronautical applications),
- Carbon/Epoxy HM composite: similar to the Al-Cu alloy, the minimum of the tensile or compression strength limit should be considered. Hence, referring to the values in section 3.3, the ultimate compressive stress is considered (SF=1.5 is also used).

Table 4 – Maximum allowable stress values for the Al-Cu alloy and carbon/epoxy composite.

Material	Maximum allowable stress (MPa)
Serie 2024T3 Al-Cu alloy	230
HM Carbon/epoxy composite	450

Evaluating a precise value for maximum strain is not as simple as that of stress. There is no sufficient literature regarding the topic for a small/medium-sized LTA platform. However, it is reasonable to think in terms of aerodynamic forces whose values depend a lot on the airship slenderness and its variation due to the deformation of the main rib. Here, it is useful to consider Hoerner's semiempirical relations [10] between the aerodynamic drag coefficient (C_d) and the slenderness (*L/d*) of the airship. A C_d minimum can be found for a slenderness value of 4.6. Higher values of slenderness decrease the airship volume available to store gas and consequently reduces buoyancy. So, for the current airship design, a *L/*d value of 3 is used, as a compromise between buoyancy and drag.

To establish a maximum strain value, a typical length of 30 m for the airship major axis is considered. Assuming rib displacements of around 0.5 m and 1 m, the slenderness varies by -9% and -16.17%, respectively. Even if a 0.5 m displacement limit guarantees better aerodynamic performance, the increase in structural weight to obtain it must be considered. For this reason, the choice of material is fundamental to containing the strain of the structure without excessively increasing the weight, thus facilitating airship hovering using only buoyancy loads to support the airship weight.

4. Analysis & Results

The structural behaviour of the airship was analysed using a finite element model of the airship structural frame in ABAQUS [11]. For this preliminary design, only the rib was modelled (since it represents the primary structural member), while the masses of the various airship subsystems were assumed to be point masses connected at various locations of the rib using rigid links. The loads and boundary conditions corresponding to the various airship operating conditions are discussed below. More complicated finite element analyses, such as the ones described in [12] and [4], are deferred to future works.

For simulating the mid-air manoeuvres of the airship, the 'inertia relief' [13] condition was used. An inertia relief analysis does not require a set of kinematic constraints to simulate the mid-air stationing of the airship. Instead, it builds a self-balanced physical system consisting of the following loads:

- Gravity loads acting on the rib and point masses,
- Inertia loads acting on the rib and various point masses,
- Buoyancy loads due to the lifting gas, applied as a distributed load on the rib.

The buoyancy load *B* [3] is directly proportional to the enclosed lifting gas volume of the airship. In the present model, the buoyancy loads are calculated and applied as a distributed load on the upper surface of the rib. To obtain a more refined distribution of the loads applied on the rib, the envelope volume was divided into different sections, each with its own volume. The volume and buoyancy load in each subdivided section '*i'* can be related to the total load and volume through the relation,

$$B_i / B_{tot} = Vol_i / Vol_{tot} \qquad (1)$$

The finer the subdivision, the better the approximation of the load distribution due to buoyancy along the rib. For the present analysis, the enclosed gas volume was divided into three sections: a central section, and two symmetrical lateral ones. Based on the value of the enclosed volume, the distributed loads *TLoad$_l$*, *TLoad$_m$* and *TLoad$_r$* were calculated for the left, middle and right sections, respectively (see Figure 4).
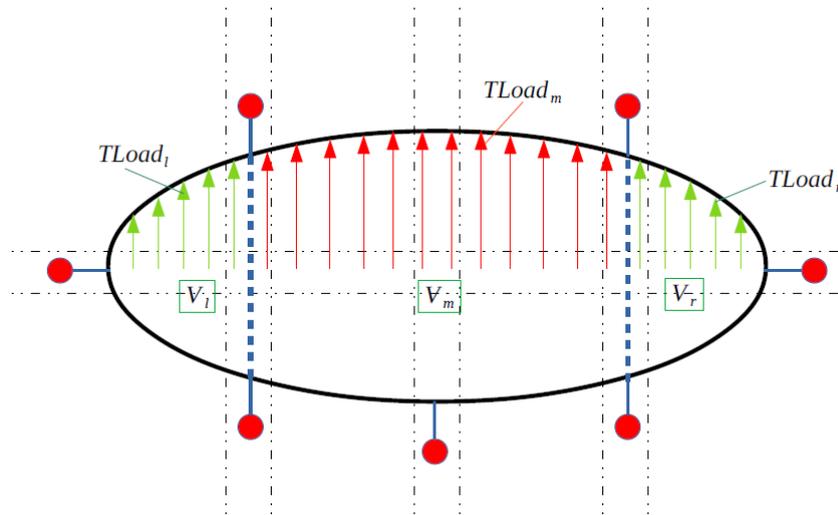
Figure 4 - Illustration of the airship model used for mid-air operations.

External air density (which is a function of altitude) also affects the buoyancy calculation. For the present analysis, an altitude of 500 m (above mean sea level) was chosen as a compromise between data acquisition quality and flight safety.

For analysing the parking and crash cases, as the airship is resting on the ground, the inertia relief condition is not required. Here, the airship is supported using two landing legs, symmetric with respect to the airship minor axis and positioned on the bottom surface of the rib (See Figure 5). The landing legs are assumed to be rigid and their connection with the rib is modelled as a fixed boundary condition at the leg location. No buoyancy loads are applied to the structure. Structural behaviour is analysed considering only the weights of the various sub-systems (structure, payload, on-board systems, engines, etc.).
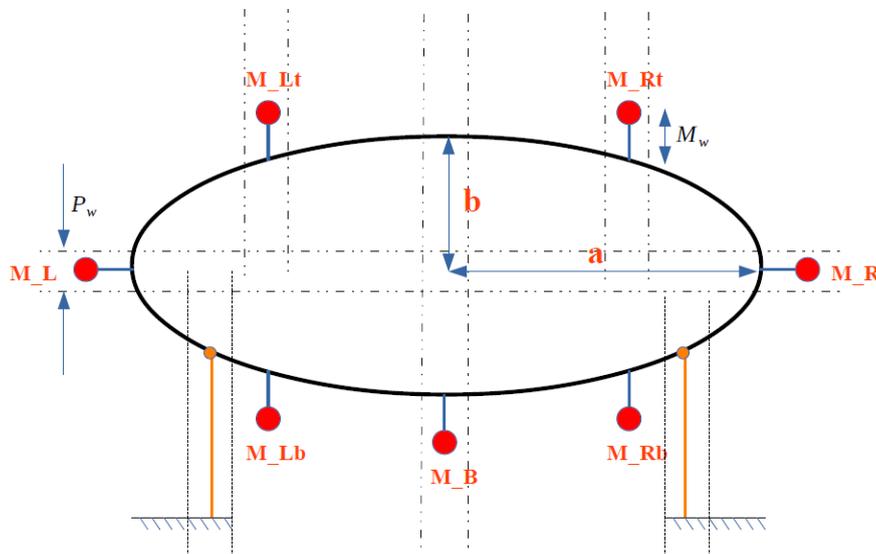

Figure 5 – Illustration of the airship model used for the parking and crash case.

It should be noted that the current structural analysis considers a very simplistic representation of the landing legs. A more accurate model would require a full structural analysis of the legs themselves and their interaction with both the ground and the rib structure. However, such an analysis does not fall within the scope of this study. A model with fixed supports and infinitely stiff legs is acceptable as a first approximation.

The structural model adopted for the analysis includes multiple parameters representing the weights of the various airship subsystems and thrusts developed by the different propellers (see Figure 6):

- $M\_Lt, M\_Rt, M\_Lb, M\_Rb, M\_L, M\_R$: masses of the propulsion systems,
- M_B: mass of the payload and on-board systems,
- $H_{Rt}, H_{Lt}, H_{Rb}, H_{Lb}, V_L, V_R$: horizontal and vertical thrusts developed by the propellers.
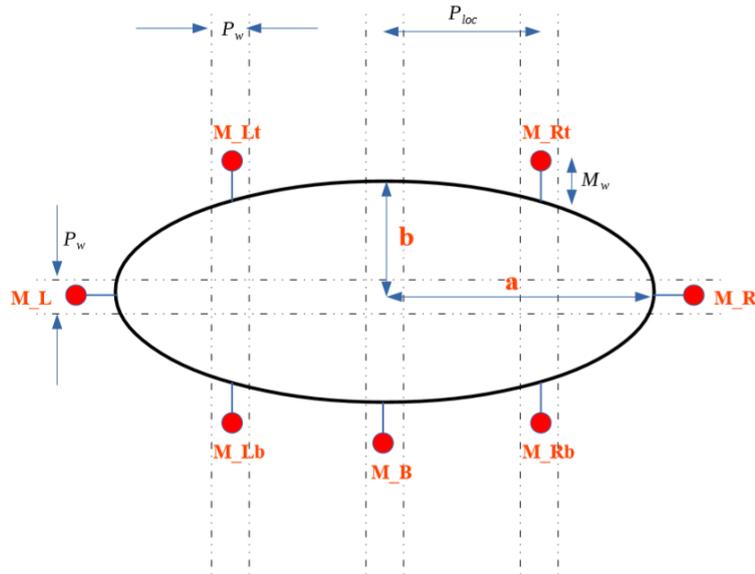
9

Figure 6 – Geometrical and dynamical parameters of the structure.

Some additional geometrical parameters controlling the location, hub assembly of the landing legs and the propulsion systems have also been introduced (see Figure 6). To keep the optimal geometrical proportions throughout all the analyses some of the parameters have been made a function of airship length L and rib section width w,

$$a = \frac{L}{2} \tag{2.a}$$

$$b = \frac{a}{3} \tag{2.b}$$

$$h = \frac{w}{2} \tag{2.c}$$

$$t = \frac{w}{40} \tag{2.d}$$

$$P_{loc} = 0.6 \cdot a \tag{2.e}$$

$$M_w = 0.03 \cdot a \tag{2.f}$$

4.1 Hovering

The hovering condition is analysed first, where the LTA platform maintains mid-air equilibrium solely under buoyancy loads without the use of propellers. No electric power is therefore required. The FE model uses inertia relief to simulate this condition (as previously discussed). The only loads on the structure are due to the weight of the structure and various subsystems, and airship buoyancy.

Two parameters are used for initial airship sizing:

- Airship length L: three sample lengths of 26, 30, 34 m are considered. These are reasonable values for a platform aimed at environmental monitoring,
- The rib section parameter, w.

Structural analysis is carried out for all three lengths, first using the Aluminium alloy, and then the HM composite rib. For each length two section dimensions (defined by w) are found:

- guaranteeing structural limits, i.e., maximum acceptable stress and displacement,
- guaranteeing vertical static equilibrium, i.e., when the buoyancy load is equal to the total weight of the airship (a tolerance of 0.5% was introduced considering situations where buoyancy loads exceed the airship weight; the ratio between exceeding lift and buoyancy should be <0.5%)

10

Table 5 – Results of the airship hovering analysis for an Al-Cu alloy rib.

L [m]	w [m]	Structural mass[kg]	Max. displacement [cm]	Max. stress [MPa]	Buoyancy [N]	Lift [N]
26	0.205	1285.7	96.2	132.9	9901	**-8110**
26	0.122	455.5	**1160**	**1050**	9901	42.1
30	0.245	2118.8	98.1	130.1	15210	**-10963**
30	0.168	996.7	**535**	**425.2**	15210	33.8
34	0.289	3341.1	98.1	119.0	22141	**-16030**
34	0.206	1698.14	**434**	**354.5**	22141	88.2

Table 5 presents the results of the hovering analysis using an Al-Cu alloy rib; all of the values which exceed the failure conditions or do not guarantee vertical equilibrium have been highlighted with bold characters. Considering the maximum acceptable stress and displacement on the rib, it is clear that those solutions which guarantee vertical equilibrium exceed structural limits, i.e., the structure is not strong and rigid enough to sustain itself without failure. Such solutions are of no interest. Even when considering solutions that fulfil the structural limits (i.e., the lightest ones to successfully sustain structural loads), they are still too heavy to perform hovering.
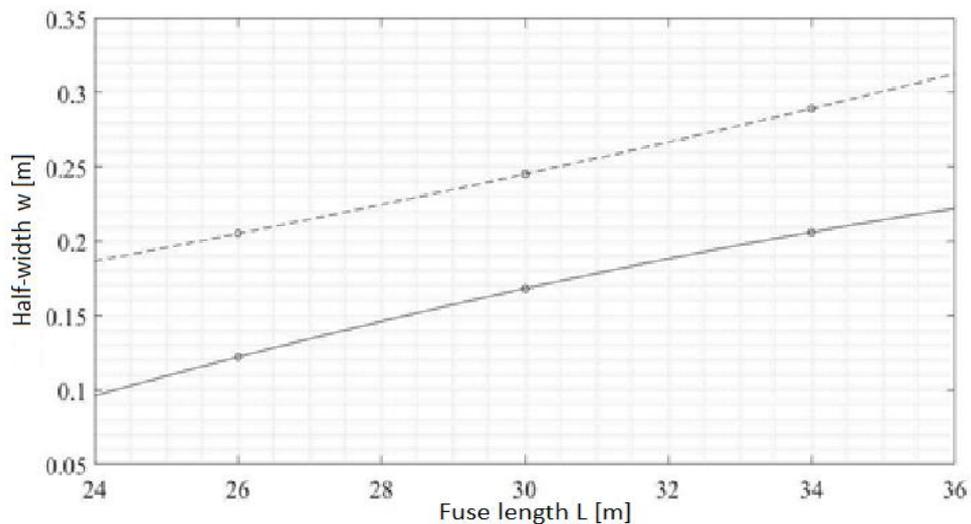

Figure 7 – Values of L and w guaranteeing vertical equilibrium solutions (continuous line), and structural limit solutions (dashed line) for an Al-Cu alloy rib.

Figure 7 shows w trends for both solutions. Note that there is no intersection and structural limits solutions are always above the vertical equilibrium solutions. Hence, Aluminium alloys are not suitable material choices. Next, airship hovering using a composite rib is analysed and the results are presented in Table 6, in which the values that exceed the failure conditions or do not guarantee vertical equilibrium have been highlighted in bold.

Table 6 – Results of the airship hovering analysis for a composite rib.

L [m]	w [m]	Structural mass [kg]	Max. displacement [cm]	Max Stress [MPa]	Buoyancy [N]	Lift [N]
26	0.165	449.5	**175**	270.5	9901	91.1
26	0.190	596.2	95.2	178.0	9901	**-1341**
30	0.225	964.3	98.1	170.0	15210	358
34	0.266	1527.38	97.7	177.8	22141	1762
34	0.280	1692.3	79.8	150.2	22141	147

These results show that no solutions under 26 m are acceptable: large rib sections are too heavy for the airship to perform hovering, while small sections make the rib unable to sustain structural loads. If airship length is increased, operative solutions are found. For lengths greater than 30 m, solutions exist which provide both acceptable structural displacements and allow airship hovering. A suitable section dimension can be chosen between the two solutions. If boarding capacity is to be preferred, a smaller section can be chosen, and the rib approaches its structural limit.
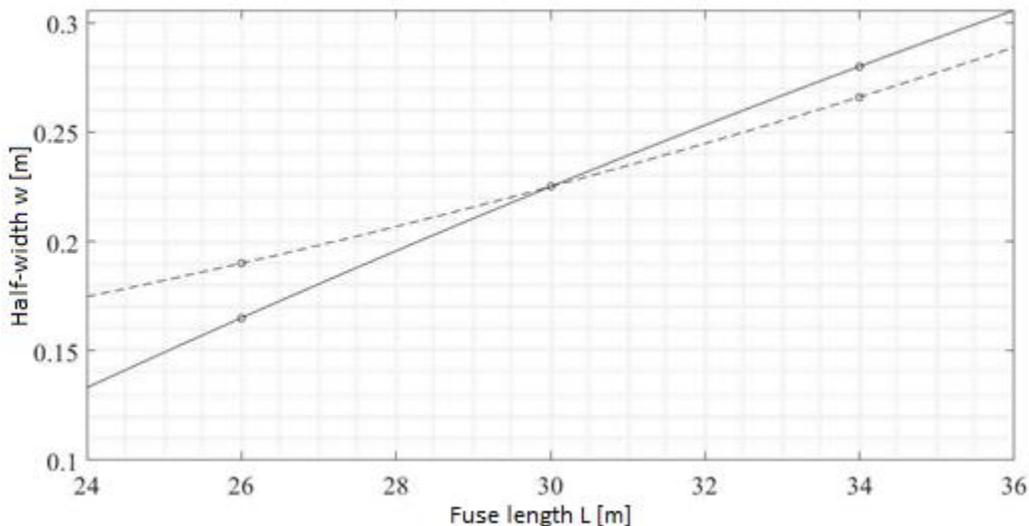

Figure 8 - Values of *L* and *w* guaranteeing vertical equilibrium solutions (continuous line), and structural limit solutions (dashed line) for a composite rib.

Figure 8 shows the trends for both solutions. An intersection occurs at *L*=30 m. For *L*<30 m there are no working solutions, while for *L*>30 m the two curves define a region in which there exist multiple possible solutions for *L* and *w*. Design solutions which fall within this region are both light enough and can sustain the structural loads to successfully perform hovering. *L*=30 m is not the exact intersection point, as it was determined through empirical iterations, but is a reasonable approximation of the real value. Figure 9 plots excess lift as a function of airship length. Intersection with the y-axis is the transition between the non-operative and the operative region. The value of *L* at the transition point (indicated by the dashed line) is between 29 and 30 m, thus confirming what stated previously.
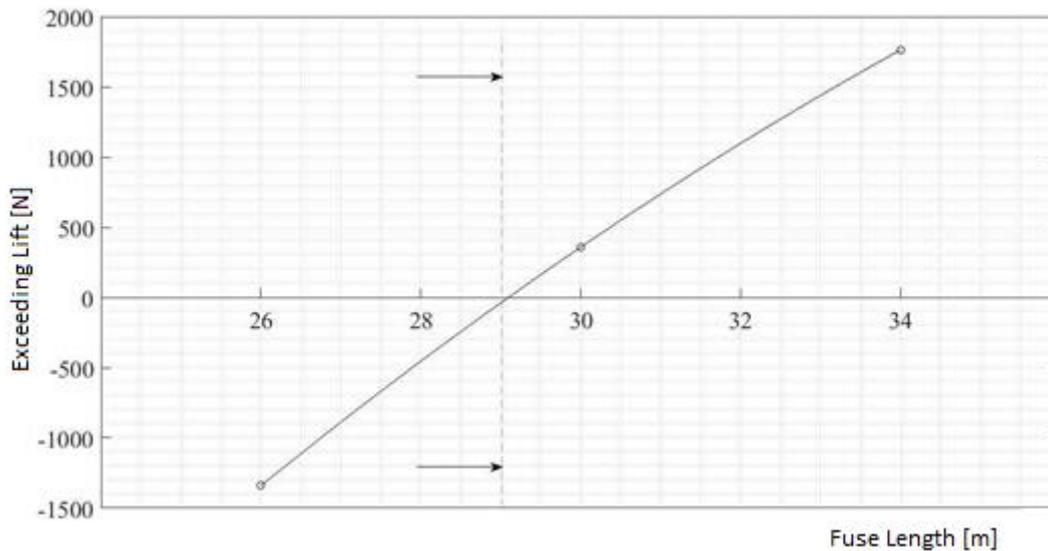
Figure 9 – Plot of excess lift generated by the airship as a function of airship length.

4.2 Parking & Crash

The present section addresses the parking and crash analyses of the airship, where it is stationed on two supports with fully inflated ballonets and no propeller thrust is applied to the structure. For this case, the FE model of the airship does not require the inertia relief condition and two simple fixed supports are introduced to simulate the two landing legs (assumed to be infinitely stiff).

Starting from the results of the hovering analysis (airship length L=30m, half-width w=0.245 m for the Al-Cu alloy, and 0.225 m for the composite), three main goals are set for the analysis:

- Assessment of the optimal position of the landing legs,
- Evaluation of the structural response and eventual increase of the section (if required),
- Performance comparison between Al-Cu alloy and carbon/epoxy composite materials.

The position of the landing legs is constrained by the propulsion system mounted on the lower surface of the rib. As this system is mounted at a distance of 0.6a from the ellipse minor axis, a lower limit of 0.65a has been set for the landing leg position. Similarly, an upper limit of 0.95a is set to avoid conflict with the propellers at the end. The change in structural response as the landing leg position is iterated between 0.65a and 0.95a (from the minor axis of the ellipse) is analysed to identify an optimum location for the landing legs. Four different positions are analysed: 0.65a, 0.75a, 0.85a, and 0.95a. Tables 7 and 8 summarize the results for the Al-Cu alloy and composite rib, respectively.

Table 7 – Results of the airship parking analysis for an Al-Cu alloy rib.

Length [m]	w [m]	% Legs	Displacement [cm]	Max Stress [MPa]
30	0.245	65	59.19	99.1
		75	42.29	84.74
		85	27.59	69.52
		95	13.28	51.56

Table 8 – Results of the airship parking analysis for a composite rib.

Length[m]	w [m]	% Legs	Displacement [cm]	Max Stress [MPa]
30	0.225	65	30.18	54.07
		75	23.37	40.62
		85	15.64	32.28
		95	7.85	28.07

It should be noted that no enlargement of the rib cross-section is required to meet the structural requirements; therefore, the parking case study does not exceed the limits imposed for the structure's safety and hence is not a limiting case. The maximum displacement and Von Mises stress have been plotted and can be found in Figures 10 and 11.
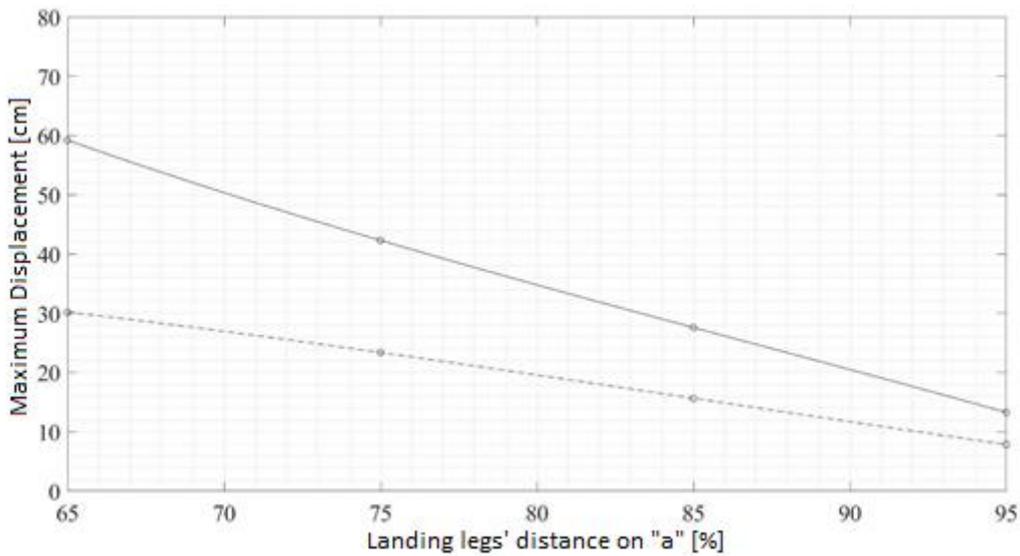

Figure 10- Variation of maximum displacement as a function of landing leg position for an Al-Cu alloy (continuous line), and composite (dotted line) rib.
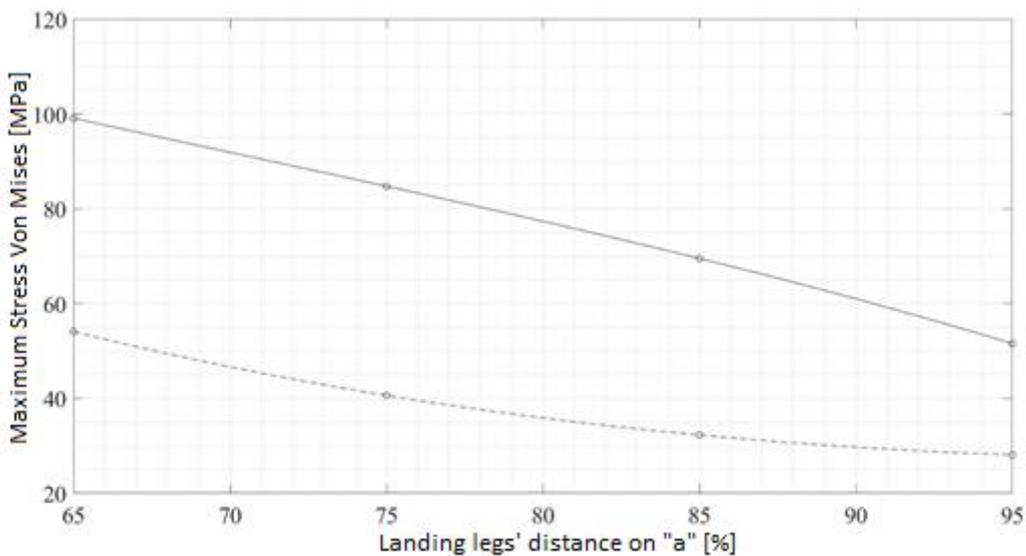

Figure 11 - Variation of maximum Von-Mises stress as a function of landing leg position for an Al-Cu alloy (continuous line), and composite (dotted line) rib.

Two main conclusions can be deduced from these analyses:

14

- both maximum displacement and maximum stress decreases as the distance between the landing legs increases, and
- the HM composite (dotted lines) is confirmed to be more performant than the Al-Cu alloy in minimizing both stresses and deformations and it results in a far lighter structure (964.3 kg vs 2118.8 kg)

A composite rib with the same cross-section width as the one obtained through the hovering analysis, and legs at the maximum possible distance is the optimal configuration for the airship in parking mode. However, legs excessively near to the vertical thrusters might result in manufacturing and integration difficulties; a leg position of 0.9*a* is taken as the optimal value and will be carried on to the next analysis.

The crash condition takes into consideration a ground impact simulation of the aircraft. The FE model and the structural dimensions are similar to those used for the parking case, with the legs at 0.9a. The unmanned airship falls in the UAS Certified Category, for which the European legislation is currently being finalised [14]. Hence, no specific regulations exist at present regarding the crash simulation. For the present analysis, a 3·g acceleration is applied to the masses of the structure (29.43 m/s^2) to simulate the accelerations involved. The results of the crash analysis show that the structural response, even if amplified, is similar to the parking results for both Al-Cu alloy and HM composite ribs (see Table 9).

Table 9 – Results of the airship crash analysis.

L [m]	*w* [m]	Landing leg position	Max. displacement [cm]	Max Stress [MPa]
30	0.245 (Al)	0.9*a*	62.09	185.1
	0.225 (HM)		35.85	90.89

As in the parking case, no enlargement of the rib cross-section is required to meet the structural requirements; therefore, the crash case also does not exceed the limits imposed for the structure's safety and is not a limiting case.

4.3 Manoeuvres with Thrusters & Control System Failure

The present section considers ordinary manoeuvres and control system failure scenarios. The six thrusters when operational and properly oriented permit efficient manoeuvres also at low flight speeds. A similar model to that used in the hovering case is employed here. In addition, to simulate the manoeuvres, propeller thrusts were also used; thrust values were set to 1000 N or 0 N depending on the case analyzed. Analyses have been carried out considering the structural dimensions obtained in the results of section 4.1: *L* = 30 m, *w* = 0.245 m (Al-Cu alloy rib), or *w* = 0.225m (composite rib). If stress rather than strain exceeds the superior limit allowed, increasing *w* could be a solution, but the consequent increase in airship mass should also be evaluated to maintain hovering capability. Even though it is already known that the Al alloy structure is not capable of performing the hovering flight, some cases with this material are discussed in this section for a comparison with the composite ones.

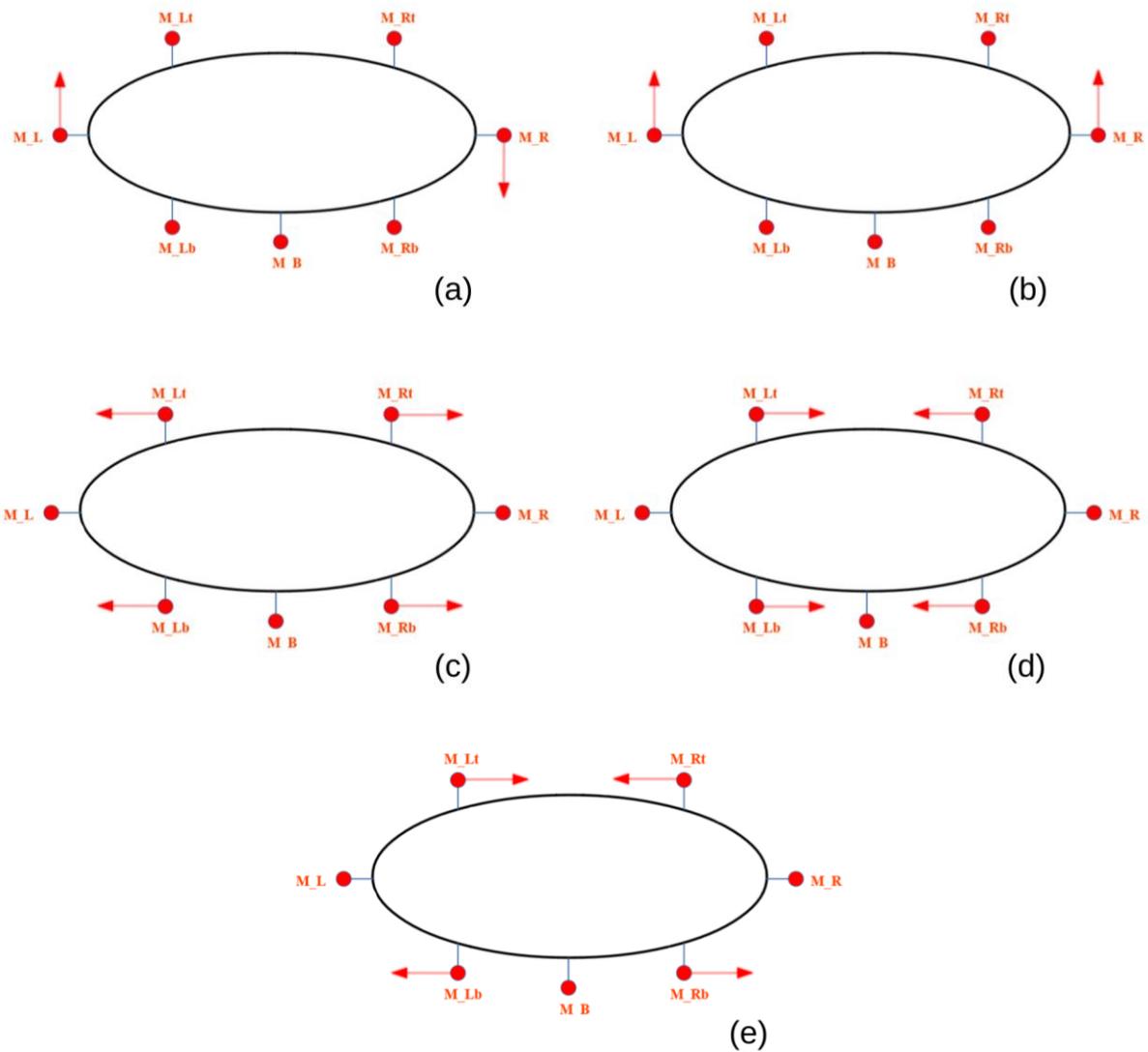The various manoeuvres considered are (as shown in Figure 12):

Figure 12 – Illustration of the various airship manoeuvres: (a) pitch, (b) descent, (c) traction-inducing failure, (d) compression-inducing failure, (e) flexure-inducing Failure.

The considered manoeuvres include:
(a) Pitch manoeuvre: vertical thrusters are switched on with loads V_L and V_R acting in opposite directions. This manoeuvre is symmetric due to the structure and loads' disposition symmetry.
(b) Vertical descent: vertical thrusters are switched on with loads V_L and V_R acting in the same direction.
(c) Traction-inducing failure: vectoring thrusters are switched on above and under the rib and are pushing in opposite directions causing traction on the central part of the rib. This may be due to a failure in the vectoring control system.
(d) Compression-inducing failure: vectoring thrusters are switched on above and under the rib and are pushing in opposite directions causing compression in the central part of the rib. This may be due to a failure in the vectoring control system.
(e) Flexure-inducing Failure: vectoring thrusters are switched on above and under the rib and are pushing in opposite directions causing compression on the upper part of the rib and traction on the lower part of it. This may be due to a failure in the vectoring control system.

Table 10 – Results of the airship manoeuvring analysis for an Al-Cu alloy rib.

	Pitch	Descent	Traction	Compression	Flection
Max. displacement [cm]	98.17	99.70	96.90	99.38	98.50
Max stress [MPa]	130.4	131.0	129.4	130.8	130.3

Table 10 summarizes the results for the Al-Cu alloy rib (L = 30m, w =0.245). Both stress and displacements are lower than the superior limits found in previous analyses. The most critical zones are located on the higher part of the rib and slightly shifted from the centre in the case of an asymmetric manoeuvre such as pitch. As described at the beginning of this paragraph, structural and flight conditions are simultaneously satisfied by the Al-alloy, but it is interesting to note that the most critical case is the vertical descent.

Table 11 sums up the results for a composite rib (L = 30m, w =0.225). The values that exceed the failure conditions have been highlighted in bold.

Table 11 – Results of the airship manoeuvring analysis for a composite rib.

	Pitch	Descent	Traction	Compression	Flection
Max. displacement [cm]	98.10	**101.00**	97.06	99.12	98.34
Max. stress [MPa]	171.0	175.0	169.4	170.9	170.3

Both stress and displacement are again lower than the superior limits found in previous analyses. The only exception, highlighted in red, is represented by the displacement in the most critical case, that is vertical descent (similar for the Al-alloy rib). Although the displacement exceeds the superior limit by a 1% factor, considering the approximate methods used to determine the limit, it was decided not to increase the w of the section and consequently the rib mass.

4.4 Optimal rib cross-section

Further analyses have been conducted to dimension the structure and to ensure that it is capable of sustaining the most critical manoeuvring conditions (vertical descent). The carbon/epoxy HM rib was chosen as it is the only one that led to acceptable solutions in the hovering case study. Three different configurations with airship lengths of 30, 32 and 34 m are considered, and the results are shown in Table 12, in which the values that exceed the failure conditions have been highlighted with bold characters.

Table 12 – Optimal rib cross-sections for various airship lengths.

L [m]	w optimum [m]	Struct. mass [kg]	Max. displacement [cm]	Max Stress [MPa]	Buoyancy [N]	Lift [N]
30	0.225	964.3	**101.0**	175.7	15210	358
32	0.244	1209.6	**100.4**	171.8	18459	1194
34	0.266	1527.38	99.2	180.9	22141	1762

Yet again, the rib section identified during the hovering analysis is found to be the optimal solution and an enlargement of the section is not required; the maximum stress is thus within the limits in all of the cases and the displacement exceeds the limits by only 1%. The lift is positive in the three cases and it increases with the airship length; the convenience of greater dimensions is therefore confirmed, and it is not surprising as buoyancy is directly proportional to the lifting gas volume, and the airship volume varies with the cube of the length.

Results found for each of the three sections can be easily interpolated, to obtain some useful first approximation relations between design parameters. Two of these expressions are particularly meaningful and allow us to link:

- airship length L to optimum structural mass, P, fulfilling both maximum displacement requirements and positive lift,
- airship length L to optimum section width w.

The interpolation polynomial is assumed to be quadratic. Such interpolation is not valid under 30 m and is poor in accuracy over 36 m. This does not pose an actual problem though: over such lengths building and transportation management-related costs would be too large for the platform to be cost-effective. The length range should be within the project feasibility.
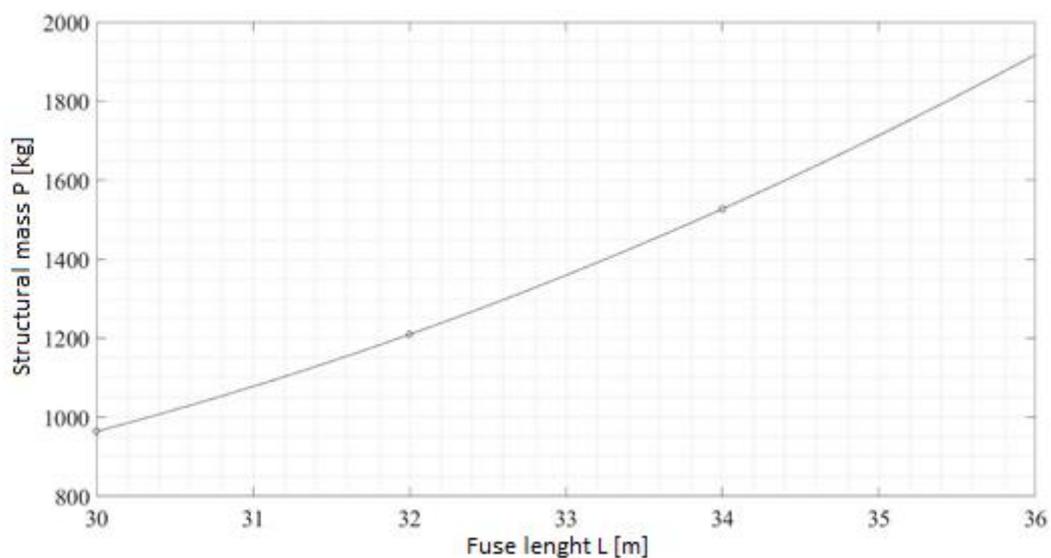

Figure 13 – Variation of structural mass as a function of airship length.
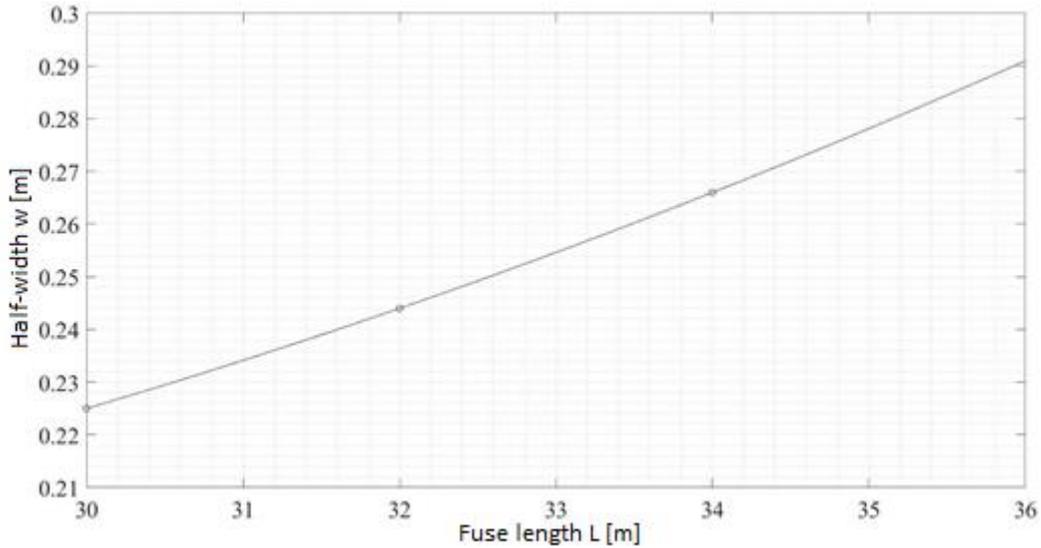
Figure 14 – Variation of optimal rib section width as a function of airship length.

The interpolation leads to two closed-form equations, suited for this specific case study (i.e., not generalised functions), which could easily be implemented in an iterative algorithm for the sizing of an airship:

$$P = 9.06 \cdot L^2 - 439.07 \cdot L + 5982.4 \qquad (3.a)$$

$$w = 0.000375 \cdot L^2 - 0.01375 \cdot L + 0.3 \qquad (3.b)$$

These equations are plotted in Figure 13 and 14.

Nevertheless, it is necessary to remember the limits in the field of application:

● Fuse length between 30 m (vertical static equilibrium limit) and 34 m,
● Structure made of Carbon/Epoxy HM and with the adopted geometry,
● Maximum acceptable displacement of 100 cm

Based on the results of the structural analysis, the final range of acceptable geometrical dimensions for the proposed LTA platform (with a composite rib), their corresponding structural weight, and buoyancy generated is reported in Table 13. Please note that the parabolic approximation returned acceptable results between 30 and 36 m, which therefore are the limits of validity. However, considering all the other structural and non-structural factors (described in detail in [1]), this range was further restricted between 30 and 34 m.

Table 13 – Ranges of values for the geometrical and performance parameters of the airship proposed.

L [m]	w [m]	Weight [kg]	Buoyancy [N]
30	0.225	964	15210
32	0.244	1210	18458
34	0.280	1527	22141

5. Conclusions

This work explored the structural design aspects of a Remotely Piloted Aircraft System concept for land survey applications. The main structural frame of the airship consists of an elliptical rib with a bi-cell cross-section. The structural behaviour under various nominal and failure operational conditions were analysed, and the performance of different rib materials were also investigated. The design process aimed at sizing the rib geometry to withstand the various operational loads, limiting structural deformations, and ensuring that the operational requirements of the airship were satisfied. Based on the results from several analyses, it was concluded that the Carbon/Epoxy HM composite is the ideal material candidate for the proposed airship prototype, with an airship length in the range of 30 to 36 m capable of satisfying the structural safety requirements and guaranteeing mid-air vertical equilibrium (further reduced in the 30-34 m to comply with non-structural needs).

The maximum displacement found in the solutions, while being under the acceptable set value (1 m), is however too great and impractical for the actual project (which has several other non-structural related requirements). The current rib cross-section, as presented in the paper, is prone to large displacements even when Carbon/Epoxy HM composite is adopted. Therefore some further changes must be considered in the design. These changes are aimed at obtaining a stiffer rib without adding weight to the section by thickening it, thus achieving lower displacements. Moreover, the local strain on the structure has not proved to be an issue when it comes to structural integrity, so a thicker section would also be pointless.

To avoid designing a new section from scratch for achieving the objectives stated above, two alternative solutions are hereafter proposed:

- To introduce additional geometry elements to the section to increase the moment of inertia, thus limiting flexure when loaded and decreasing displacements,
- To introduce new structural elements, such as tie rods, on the rib plane.

Future work will focus on investigating the use of these alternative solutions.

6. Contact Author Email Address

Mail to: rinto.roy@polito.it

7. Copyright Statement

8. Acknowledgements

References

[1] Surace C, Civera M, Roy R, Bertolotti S C, Cosenza D, Gili A, and Gili P. Design of a prototype unmanned lighter-than-air platform for remote sensing: control, alimentation, and propulsion systems. Presented at the *32nd congress of the International Council of the Aeronautical Sciences (ICAS)*, Shanghai, China, 2021.

[2] Elfes A, Bueno S S, Bergerman M and Ramos J G. A semi-autonomous robotic airship for environmental monitoring missions. In: Proceedings. *1998 IEEE International Conference on Robotics and Automation* (Cat. No. 98CH36146). Vol. 4. IEEE. 1998, pp. 3449–3455.

[3] Manuela Battipede and Piero Gili. Gli aeromobili più leggeri dell'aria. Technical Report. 2002.

[4] Cappadona A, Lecca R, Vazzola M, Gili P, Farina P and Surace C. Innovative unmanned airship structural analysis: Dual-hull and exoskeletal configurations. In: *J. Phys.: Conf. Ser*. Vol. 181. 2009, p. 012097.

[5] Porta M. Subsystems mass estimation of a UAV-LTA stratospheric platform. Master Thesis in Aerospace Engineering, Politecnico di Torino (2016).

[6] Matweb. Aluminium 2024-T3. 2016. url: http://www.matweb.com/search/DataSheet.aspx?MatGUID=

57483b4d782940faaf12964a1821fb61&ckck=1.

[7] Matweb. Online Materials Information Resource. 1996. url: http://www.matweb.com/.

[8] Civera M, Boscato G and Fragonara, L Z. Treed Gaussian Process for manufacturing imperfection identification of pultruded GFRP thin-walled profile. *Composite Structures*, Vol. 254, p 112882, 2020.

[9] Boscato G, Civera M, and Fragonara, L Z. Recursive Partitioning and Gaussian Process Regression for the Detection and Localization of Damages on Pultruded GFRP Material. *Structural Control and Health Monitoring*. (Accepted for publication).

[10] Khoury G A. *Airship technology*. Vol. 10. Cambridge university press, 2012.

[11] Dassault Systemes Simulia Corp. Abaqus Analysis User's Guide; Dassault Systemes Simulia Corp: Providence, RI, USA, 2013

[12] Becker W, Oakley J E, Surace C, Gili P, Rowson J and Worden K. Bayesian sensitivity analysis of a nonlinear finite element model. *Mechanical Systems and Signal Processing*, Vol 32, pp 18-31, 2012.

[13] Liao L. A study of inertia relief analysis. *AIAA 2011-2002*, In: *52nd AIAA/ASME/ASCE/AHS/ASC Structures, Structural Dynamics and Materials Conference,* Denver, Colorado, USA, 2011.

[14] EASA. Commission Implementing Regulation (EU) 2019/947. 2019. url: https://www.easa.europa.eu/document-library/regulations/commission-implementingregulation-eu-2019947.